Quaternary Science Reviews 344 (2024) 108981

Contents lists available at ScienceDirect

Quaternary Science Reviews

journal homepage: www.elsevier.com/locate/quascirev

Hydroclimate modulation of central-eastern Mexico by the North Atlantic subtropical high since the little ice age

Patricia Piacsek [a,*], Juan Pablo Bernal [a], María del Pilar Aliaga-Campuzano [a], Luis Bernardo Chavero [a], Fernanda Lases-Hernández [b], Francisco William da Cruz [c], Nicolás Misailidis Strikís [c,d], Liliana Corona-Martinez [a], Veronica M. Ramirez [c], Marília Harumi Shimizu [e], Herminio Rojas [f]

[a] Instituto de Geociencias, Universidad Nacional Autónoma de México, Campus UNAM Juriquilla, Querétaro, Qro, 76230, Mexico
[b] Facultad de Química, Universidad Nacional Autónoma de México, Unidad de Química en Sisal, Parque Científico y Tecnológico de Yucatán, Mérida, YUC, Mexico
[c] Instituto de Geociências, Universidade de São Paulo (USP), São Paulo, Brazil
[d] Departamento de Geoquímica, Universidade Federal Fluminense, Niterói, 24020-141, Brazil
[e] Instituto Nacional de Pesquisas Espaciais (INPE), Brazil
[f] Xkit Turismo Aventura, Zapotitlán de Méndez, Puebla, Mexico

ARTICLE INFO

Keywords:
LIA and HI
NASH
NAO
ENSO
Hydroclimate
Pseudokarstic cave
Eastern Mexico

ABSTRACT

We reconstructed the hydroclimate of central-eastern Mexico over the last 700 common era (CE) based on inferences from multi-proxies from a stalagmite (K-Inc) collected at Karmidas cave, eastern México. Projections on hydroclimate variability in Mexico raise concerns about possible future occurrences of severe droughts and seasonal water balance fluctuations related to increased global temperatures caused by anthropogenic climate change (Murray-Tortarolo, 2021). The eastern region influences the production and supply of food to Mexico. Simulations of past climates, validated by paleoclimate records, yield valuable perspectives on climate change and enhance our understanding of future projections. However, the paucity of paleoclimatic records hinders understanding past hydroclimatic variations and their climatic mechanisms in eastern Mexico. Our record covers the Little Ice Age (LIA) through the Historical Interval (HI), a crucial period for understanding the climate repercussions spanning the transition from Earth's climatic history to the post-industrial era. The reduced intensity of the North Atlantic Subtropical High (NASH) during the LIA enabled a prominent negative phase of NAO-like variability from 1600 CE until the end of LIA. Consequently, preferent meridional airflow within the continent fosters the encounter of moisture-laden intrusions with the increased frequency of cold surges as the occurrence of frontal rain in eastern Mexico, impairing the amount effect on the K-Inc $\delta^{18}O$ record. However, after the artificial opening of the cave in 1910 CE, the $\delta^{18}O$ records of K-Inc began to exhibit a ~20-year oscillatory periodicity. In this context, the trace elements of K-Inc help elucidate the climatic conditions that governed the precipitation regime during the investigated period. The visual alignment between the zonal sea surface temperature (SST) variability in the eastern equatorial Pacific (EEP) and the trace elements (Sr/Ca and Ba/Ca) of K-Inc reveals their relationship. Warm zonal SST in the EEP appears to be associated with changes in the length of the winter and summer seasons in eastern Mexico during the LIA. In contrast, over the HI, the trace elements of K-Inc show an anti-phase response to Warm zonal SST in the EEP, denoting wetter climate conditions at the vicinities of Karmidas Cave. This configuration led to questioning the influence of SST zonal variability in the EEP during the HI, which was probably masked by more relevant climate forcing. Our findings enabled us to draw climate scenarios by addressing the main climate drivers in our records.

* Corresponding author.
E-mail address: piacsekpatricia@geociencias.unam.mx (P. Piacsek).

https://doi.org/10.1016/j.quascirev.2024.108981
Received 7 January 2024; Received in revised form 11 September 2024; Accepted 18 September 2024
Available online 16 October 2024

1. Introduction

Currently, more than 126 million people live in Mexico. Despite being a populous country, approximately half of the Mexican population lives in a narrow climate band of subtropical highlands across the country's center, representing ~20% of the entire Mexican territory (INEGI, 2020). The precipitation regime over the trans-Mexican volcanic belt (TMVB) directly impacts the quality of crop yields of both subsistence farming and industrial agriculture and the lives of many people who depend on the resources coming from this key area. The projections for the Mexican hydroclimatic variability bring concerns about the possibility of future severe droughts and more extreme seasonal water balance, as changes in seasonal contrast patterns over Mexico in face of rising global temperatures (Murray-Tortarolo, 2021). To enhance our ability to project the repercussions of forthcoming climate alterations, it becomes imperative to delve beyond meteorological records into paleoclimate archives.

The Little Ice Age (LIA) is the last significant climate change, characterized by a 1-3 °C climate fluctuation that significantly impacted preindustrialized societies. The LIA represents a pivotal intersection between the Earth's climate and human history. The LIA was preceded by a drought period that possibly propelled the mysterious abandonment of Cantona between 900 CE and 1050 C, one of the largest cities in pre-Columbian Mesoamerica (Bhattacharya et al., 2015). This temporal framework offers the opportunity to comprehend short-term climatic trends, such as those associated with the El Niño-Southern Oscillation (ENSO), influencing precipitation disparities over the past millennium. Indeed, several records have joined efforts to reconstruct the climate of central Mexico, which mainly consists of lake sediment cores (Metcalfe et al., 2010; Cuna et al., 2014; Bhattacharya et al., 2015). Despite the diverse range of proxies derived from these cores, their temporal resolution remains insufficient to capture seasonal variations. Inferences from tree-ring across Mexico revealed the seasonal soil moisture regimes since the late prehispanic era (1400–2012CE; Stahle et al., 2016) found that the precipitation regime in central Mexico has little influence from ENSO variability, attributing its oscillations mainly to sea surface temperature (SST) of Atlantic Ocean. Nevertheless, it is essential to note that ring width measurements often underestimate exceptionally wet years, commonly denoted as 'wet bias'. The manifestation and magnitude of this wet bias phenomenon exhibit variability depending on the specific tree species, geographical location, and prevailing precipitation patterns. Consequently, the complexities involved in ascertaining the underlying mechanisms of this bias make it challenging to formulate generalized explanations (Sun et al., 2017).

In this sense, stalagmites are also potentially robust paleoclimatic toolboxes providing interannual to sub-annual records of change in the

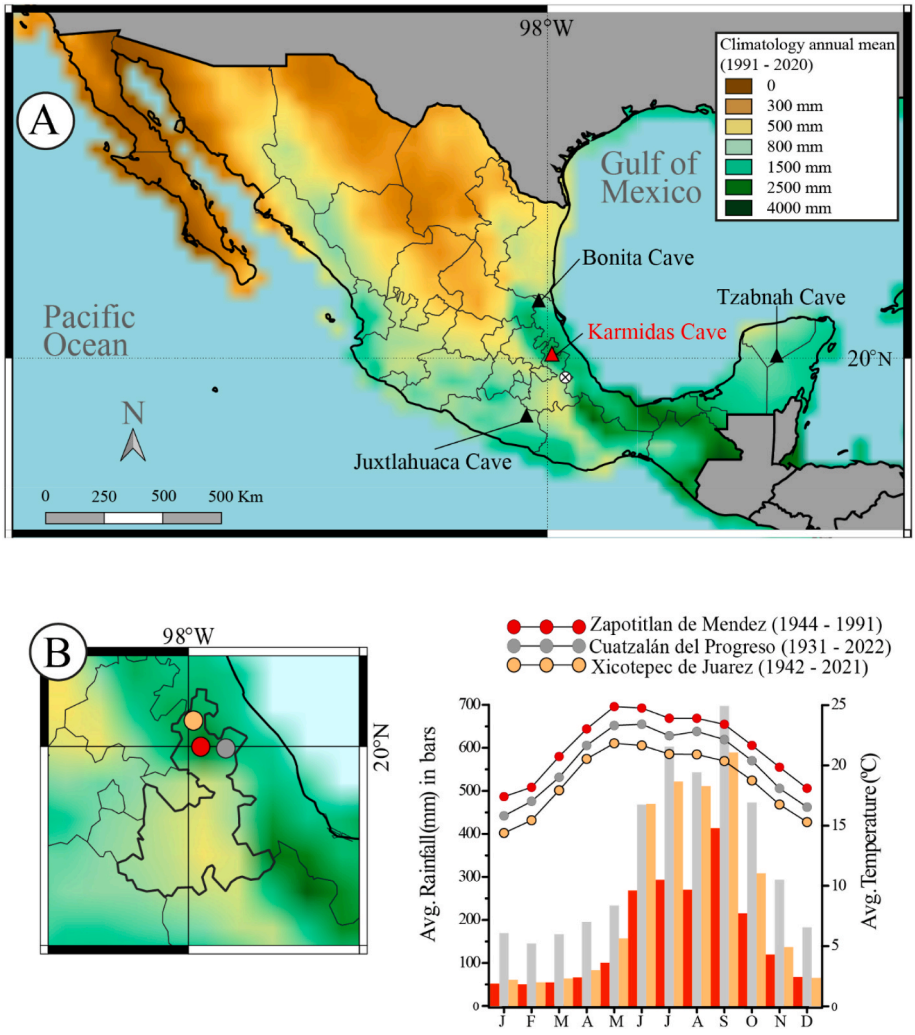

Fig. 1. (A) Map shows the mean annual rainfall from 1991 to 2021 in Mexico (Climate Change Knowledge Portal (CCKP), 2021) and location for the regional records discussed in this paper. Blue circle for lake sediment core: 1- Aljojuca maar lake (Bhattacharya et al., 2015); Triangles for stalagmites: This study (Karmidas cave) in red; Bonita cave (Wright et al., 2022); Tzabnah cave (Medina-Elizalde et al., 2010) and Juxtlahuaca Cave (Lachniet et al., 2012) in black. (B) Location for the 3 meteorological and monthly average historical variability of rainfall amount and air temperature at each (INEGI, 2020).

local precipitation regimes according to variations in the hydrogeochemistry of karst seepage solutions. Here, we present robust multiproxy inferences, with annual and sub-annual resolution, from a stalagmite that reconstructs the climate history of central-eastern Mexico since the Little Ice Age. A deep understanding of cave functioning aligned with the processes that modulate the behavior of different geochemical proxies within the stalagmite has formed the cornerstone of our paleoclimatic reasoning. The results reveal the complexity of global and regional climate forcing interactions, how different ocean-atmospheric dynamics play a role in hydroclimate, and the variability of seasonal contrast in central-eastern Mexico. This work stands as a bridge that spans the transition from Earth's climatic history to its development in the post-industrial era.

2. Study area

2.1. Geological features

The Sierra Madre Oriental is a mountain range with an average elevation of 2200 m above sea level (m.a.s.l.), and the length of the orographic axis of approximately 1300 km (km) is aligned in northwest-southeast direction covering nine states of Mexico. The Puebla state is located in the central-south of México, at the Sierra Madre Oriental, housing many ingrained small towns in its tropical evergreen and cloud forests, such as Zapotitlan de Méndez (20°N 97°71" W, ~700 m.a.s.l) (Fig. 1A). Zapotitlán de Méndez is positioned between two distinct geological formations: the Pimenta Formation and the Lower Tamaulipas Formation (Belt, 1925; Heim, 1926), where the Zempoala River seems to cross the geographical line that separates them.

The dissolution of the Pimenta Formation passes through the Karmidas Cave, generating a complex pseudokarst system that includes an ignimbrite layer and riverine sediments from the Zempoala River. According to Aliaga-Campuzano et al. (2017), about 168 (+7.7/−7.5) ka, a colossal collapse of Los Humeros Caldera filled with pyroclastic flows the surrounding ravines, reaching the deep valleys of both the Apulco and Zempoala rivers. The deposited layer of Xaltipan ignimbrite at Karmidas Cave derived from Los Humeros Caldera, placed ~45 km away from the Los Humeros hotspot (Carrasco-Núñez et al., 2018). In short, Karmidas Cave is overlaid by an upper layer of Xaltipan ignimbrite and underlain by a diamicton, attributing unique features to the pseudokarst system.

2.2. Climate setting

Air-sea interaction strengthens moisture loading from the Caribbean Sea and the Gulf of Mexico during warm and wet boreal summers, reaching the windward (eastern) side of the Sierra Madre Oriental with orographic rain (Mestas-Nuñez et al., 2007). The warmer Tropical North Atlantic, Gulf of Mexico, and Caribbean Sea SST enhance the moisture boundary layer, boosted by the threshold of SST above 28 °C (Graham and Barnett, 1987; Bhattacharya and Coats, 2020; Yun et al., 2021). The westward expansion of the North Atlantic subtropical high of Azores (NASH) is most potent in the summer. Subsequently, it enhances the easterlies, facilitating moisture intrusion into the continent in tropical latitudes. A maximum of easterly zonal wind at 925 hPa in the Caribbean region is called the Caribbean Low-Level Jet (CLLJ), which generates meridional wind anomalies from the Caribbean Sea and Gulf of Mexico to the United States. The CLLJ is a fundamental feature of the hydroclimatology over Mexico, and it is a result of teleconnection forcings between the Atlantic and Pacific Ocean basins, such as El Niño-Southern Oscillation (ENSO), the North Atlantic Oscillations (NAO), and tropical Atlantic variability (Wang, 2007). The CLLJ varies semi-annually, with two maxima in the summer and winter. By reaching its maximum in July (boreal summer), a minimum rainfall over Central America and southern Mexico operates probably due to the enhanced divergence of moisture flux in the Caribbean Sea that suppresses the convectional rain. This phenomenon is broadly known as the mid-summer drought and is also related to a minimum of tropical cyclones in the Caribbean region (Magaña et al., 1999).

Wang (2007) showed via observational data that the second peak of CLLJ is during the wintertime when the NASH is weakened, favored by the negative sea level pressure anomalies in the subtropical North Atlantic. ENSO events generally form during the spring and summer in the northern hemisphere and peak during winter. Thus, the intensity of winter CLLJ is potentially influenced by the mature phase of ENSO. During the winter, cold SST anomalies in the tropical Pacific are commonly associated with strong CLLJ. This phenomenon is also ascribed to southerly wind anomalies that carry increased moisture, resulting in enhanced rainfall across the United States and more frontal precipitation over the Caribbean Sea and Southern Mexico. Notwithstanding, weak CLLJ is associated with northerly wind anomalies, periodic low-level winds from continental polar surges known as "Nortes" that channel along the eastern side of the Sierra Madre Oriental, favoring equatorward incursion (Schultz et al., 1998), collecting abundant moisture by passing over the Gulf of Mexico and providing frontal rain in the region (Magaña et al., 2003).

Winter has lower precipitation amounts; Indeed, meteorological records spanning the period from 1944 to 1991 reveal that, on average, Zapotitlán de Méndez experiences ~1550 mm of precipitation during the summer months (May to October) and ~400 mm during the winter months (November to April). Zapotitlán de Méndez has lacked meteorological records for over 30 years. Therefore, we consulted information from neighboring cities, the furthest of which is less than 40 km away, such as Cuetzalán del Progreso (20.02°N, 97. 52°W and ~970 m.a.s.l., with records available from 1931 to 2022) and Xicotepec de Juárez (20.27°N, 97.96°W ~1170 m.a.s.l., records from 1942 to 2021). Respectively, these cities exhibit average rainfall amounts ranging from approximately 3020 mm–2400 mm during summer and between 1150 mm and 700 mm during winter. The three meteorological records exhibit a monthly covariance in the precipitation amount and substantiate rainy days for this region, even during the winter season. In the context under consideration, the precipitation regime in the vicinities of Zapotitlán de Méndez holds considerable significance throughout the year (Fig. 1B), covering a transitional strip between two physiographic provinces of Mexico: humid mountain forest and tropical humid forest (Cervantes-Zamora et al., 1990); the occurrence of this type of physiography is possible in constantly humid environments throughout the year.

3. Methods

3.1. U–Th dating

The stalagmite Karmidas-Inclined(K-Inc) was retrieved from Karmidas Cave in November 2012. The drip site (DS) was monitored, and the glass substrates were allocated in an inclined orientation to monitor recent calcite formation. Thus, the stalagmite was named Karmidas-Inclined (K-Inc) (Fig. 2). The stalagmite K-Inc is 63.30 mm long in its growth axis, cut along, and polished. Using a 1-mm diameter micromill, 5 subsamples were drilled for U–Th dating along the growth axis at 19 mm, 29 mm, 39 mm, 59 mm, and 70 mm (Fig. 2).

The U-Th dating of the samples was performed by isotope-dilution MC-ICPMS using a Thermo-Finnigan Neptune Plus at Centro de Geociencias, Universidad Nacional Autónoma de México (UNAM), following the methodologies of Hernández-Mendiola et al. (2011), but the measurement protocols modified for MC-ICP-MS using a high-purity ^{229}Th spike obtained from Oakridge National Laboratory and ^{233}U from IRMM 051a reference material. The sample was prepared in a class-100 clean lab, with blanks typically lower than 3 pg of ^{238}U and 1 pg of ^{232}Th. The samples measured produced low ^{232}Th signals (<0.01 V); no tailing corrections on ^{230}Th were necessary. All ages were calculated with Isoplot v. 3.75 (Ludwig, 2012) using half-lives for ^{238}U from Jaffey et al.

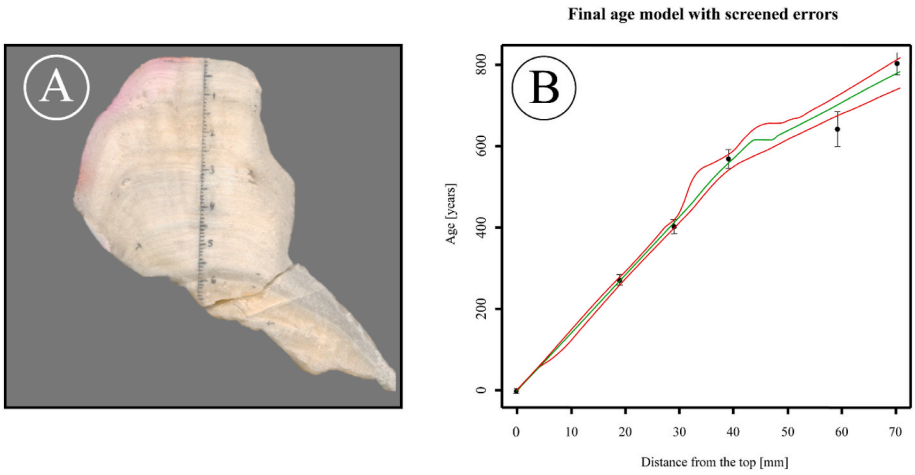

Fig. 2. The age model for the inclined stalagmite. (A) The stalagmite from Karmidas – inclined (K-Inc). (B) The age model based on $^{232}Th/^{238}U$ analysis considered zero as the first hypothetical initial age due to active calcite growth at the time of stalagmite removal in 2012.

(1971) and for ^{234}U and ^{230}Th from Cheng et al. (2013). The $^{230}Th/^{238}U$ ages were corrected for the contributions from detrital material using a two-point isochron (Ludwig and Paces, 2002), and assuming a composition of the detrital material like the crust of the Earth with $^{232}Th/^{238}U = 3.8 \pm 2.0$ (Taylor and McLennan, 1985) and within 10% of secular equilibrium; i.e $[^{234}U/^{238}U] = 1.0 \pm 0.1$ and $[^{230}Th/^{238}U] + = 1.0 \pm 0.1$ (Further details at Supplementary Table S1). All ages are in stratigraphic order and have continuously grown since ~1230 CE ± 26 with an average growth rate of 70 μm per year and little variability from sample 39 mm to the top. However, the highest growth rate was 240 μm per year between 39 and 59 mm, between 1390 and 1460 CE.

3.2. Stable isotopes

A total of 44 drip samples were collected at different locations within the cave over different seasons; details about the monitoring are provided in SI Appendix 1. The $\delta^{18}O$ and $\delta^{2}H$ composition of drip water were analyzed at Laboratorio de Análisis de Isotopos Estables at Facultad de Química, UNAM in Yucatán, Mexico, using a Gasbench II sample preparation system coupled with a Thermo Scientific Electron Delta-V PLUS IRMS. For $\delta^{2}H$ analyses, the samples were purged with a 2% H_2/He mixture and were left to equilibrate for 2 h at room temperature; then, an H_2 aliquot was extracted and analyzed. For $\delta^{18}O$ analysis, the samples were equilibrated with a 0.3% CO_2/He mixture and then left to equilibrate for 20 h at room temperature. An aliquot of the isotopically equilibrated CO_2 gas was then extracted and analyzed for its isotopic composition. The analysis of certified standards VSMOW2, GISP, and VSLAP bracketed the analysis of samples. Long-term uncertainties are 0.2‰ and 3‰ for $\delta^{18}O$ and $\delta^{2}H$, respectively. Finally, all $\delta^{18}O$ and $\delta^{2}H$ values reported here are referenced against the Vienna Standard Mean Ocean Water (Coplen, 1996).

The stalagmite K-Inc was sampled at ~300-μm intervals over the growth axis using a microdrill to extract approximately 500 μg of calcite. The $\delta^{13}C$ and $\delta^{18}O$ were measured in 672 samples using an isotope ratio mass spectrometer (IRMS) coupled to a gas bench system II at the Stable Isotopes Laboratory at the Institute of Geosciences, University of São Paulo (USP), Brazil, resulting in an average of ~1.8-yr resolution between samples. Isotope ratios are expressed in δ-notation, with per mil deviation from the Vienna Pee Dee Belemnite (VPDB) standard for carbonates, with typical uncertainties of ±0.2‰.

3.3. Trace elements (TE)

Thermo iCAP 6500 Duo View ICP-OES measured the trace elements (TE) from the drip water at Centro de Geociencias, UNAM. The analysis consisted of ten samples bracketed by an in-house cave-water standard previously characterized for its elemental composition and acid blanks. The intensity ratios were converted to elemental ratios following de Villiers et al. (2002). The TE has uncertainties of ~3%. Mg, Ca, Sr, and Ba concentrations were also calculated against IV-ICPMS-71A reference material.

The TE analyses in the stalagmites were conducted at Laboratorio de Estudios Isotopicos (LEI) in Centro de Geociencias, México. The stalagmite was analyzed for Mg/Ca, Sr/Ca, and Ba/Ca ratios using Laser Ablation Inductively Coupled Plasma Mass Spectrometry (LA-ICP-MS) using a Resonetics L-50 excimer laser-ablation workstation (ArF, $\lambda = 193$ ns, 23 ns FWHM, fluence of ~6J/Cm^2) at Centro de Geociencias, UNAM. The laser was masked and projected as a 200 × 20 μm beam onto the sample, with the larger axis of the laser beam perpendicular to the stalagmite growth axis. The sample was moved under the laser at a rate of 0.5 mm/min with a laser fluence of 3J/cm^2 and a sampling rate of 5Hz, resulting in a continuous record (Bernal et al., 2016). Trace element ratios were calculated against NIST 612 using Iolite 3.6 (Paton et al., 2011). The resulting trace element ratios records for K-Inc comprise a total of 18593 sample points, with an average resolution of ~26.5 samples per year; the stalagmite has a sub-annual resolution. The distance roamed by the laser was calculated using the log file against the laser spot size and a timestamp. This log file was imported into Iolite 3.6 and interpolated to the same sampling density as the mass spectrometry data.

4. Results

4.1. Age model

We used the StalAge code to establish the depth-age models (Scholz and Hoffmann, 2011). To run the StalAge code, we used the high-resolution depth measurements obtained through Laser Ablation Inductively Coupled Plasma Mass Spectrometry (LA-ICP-MS) at the Laboratorio de Estudios Isotópicos (LEI) within the Center of Geosciences at Universidad Nacional Autonoma de México (UNAM). We must highlight that we consistently collected recent calcite deposits in the artificial glass substrates throughout the monitoring, entailing an active deposition of calcite layers over the stalagmite. In this fashion, the sample grew until 2012 CE, when removed, generating one additional age for the age model of K-Inc. Fig. 2 shows the U–Th dating results, indicating that the segment near the top and bottom of K-Inc was deposited from ~1300 to 2012 CE, covering the entire Little Ice Age (LIA) into the current present.

4.2. Isotopic composition of local rain, drip water, and stalagmite

Tropical oceans have moist convection zones, where rainfall increases sharply by 26–28 °C (Graham and Barnett, 1987; Sud et al., 1999; Yun et al., 2021). The SST of the Gulf of Mexico and the Caribbean significantly influences the humidity of the air masses that arrive in the Sierra Madre Oriental, bringing rain. Despite this, the isotopic ratio of the rainfall at Zapotitlán de Méndez is expected to display the amount effect as the lowland areas near the Gulf of México. On this premise, we used rainwater isotopes from drip water collected between October 2007 and October 2008 at Karmidas Cave.

The data from the meteorological station of Veracruz were obtained from the Global Network of Isotopes in Precipitation of International Atomic Energy Agency (GNIP-IAEA) database and referred to the precipitation events from the 1960s to the 1980s; $\delta^{18}O$ values greater than 0 permil were likely to have been affected by secondary evaporation and were thus not used herein. The $\delta^{18}O$ ranged between 0 and -12‰ (n = 84), where summer rain presented a weighted mean of −4.5‰ and the winter rain showed a weighted mean of −2.0‰, implying that seasonality exerts significant influence on mean annual $\delta^{18}O$ values corresponding with the shifts in moisture sources (Fig. 3A), disregarding the amount effect during the winter due to predominant frontal rain. In contrast, the drip waters from Karmidas cave revealed lower isotopic variations, ranging between −4.7 and −6.8‰ for $\delta^{18}O$ and between −19.5‰ and −33.8‰ for $\delta^{2}H$ (n = 22). The $\delta^{18}O$ values of drip water at Karmidas Cave also displayed a seasonal signal with a more positive average during winter (Fig. 3B) and fell upon the local meteoric water lines (LMWL).

Moreover, under the current cave conditions, the average $\delta^{18}O$ composition for the collected drip water at K-Inc (−5.2‰ VSMOW) should yield isotopically equilibrated calcite with −5.65‰ (VPDB) according to the empirical relationship proposed by Kim and O'Neil (1997). The average obtained for the modern calcite calculated from the last 5 years of stalagmite growth agrees well (−5.5‰ VPDB) with the average obtained in the modern calcite, indicating that the calcite formed in this pseudo-karstic environment well within the standard equilibrium conditions typically observed in karstic caves and underscores that kinetic fractionation during calcite precipitation is not a dominant process influencing the $\delta^{18}O$ variability of K-Inc. In turn, and in a longer time scale perspective, the record of K-Inc presents $\delta^{18}O_{VPDB}$ values with an average of one sample per year that varies between −4.4‰ and −6.5‰. We observed a decrease of $\delta^{18}O_{VPDB}$ values (−4.5 to −6.1‰) from 1310 until 1360 CE. After which, the record shows a trend toward higher $\delta^{18}O_{VPDB}$ values, with an average of −5.4‰, and we assume that a wetter climate can be considered below this average. Although the average of $\delta^{18}O$ does not change over Historical Interval (HI) (−5.5‰), we noticed a ~20-year regular cyclicity from 1900 CE onwards.

4.3. Geochemical controls on stalagmite Mg/Ca, Sr/Ca, and Ba/Ca

This section will delve into the hydrogeochemical factors governing the trace element ratios, tracing their inheritance from the drip water to the stalagmite. The two-year mean ratio of Mg/Ca, Sr/Ca, and Ba/Ca composition of the drip water above K-Inc was 2.1×10^{-2}, 9.7×10^{-4}, and 1.8×10^{-4}, respectively. To confirm that the trace elements precipitated in calcite were in equilibrium, we calculated the trace-element values expected in calcite from partition coefficients (DMg, DSr, and DBa) by following Day and Henderson (2013) close to 2.5×10^{-3}, 3.3×10^{-5} and 1.2×10^{-5} ratios for Mg/Ca, Sr/Ca, and Ba/Ca respectively in the calcite. The mean value derived from the modern calcite (2.5×10^{-4}, 5.7×10^{-5}, 1.8×10^{-5}), obtained based on the last three years of stalagmite growth, revealed that the trace elements were well integrated at surface stalagmite, except for Mg/Ca.

The second step entails verifying whether the trace elements adhere to the thermodynamic equilibrium proposed by Sinclair (2011), where the results of trace species on the stalagmite must co-vary linearly with a slope of 0.88 ± 0.13 on the plot of the molar ratios (mol Mg/mol Ca and mol Sr/mol Ca) in the logarithm function, revealing the occurrence of prior calcite precipitation (PCP). PCP is the precipitation of calcite in the karst vadose zone and/or cavities above the cave and/or along the upper flow path above the drip water because of the CO_2 degassing. During dry periods, the reduced water recharge into the karst aquifer tends to drive PCP by inducing degassing along the water seepage solution pathway, increasing the trace element ratios of the remaining solution (Cruz et al., 2007; Sinclair, 2011; Bernal et al., 2016), The opposite is expected to occur during wet periods, connecting the variations in trace element ratios of speleothems with the variability of allogeneic recharge in the karst aquifer.

The log-log plot of Mg/Ca and Sr/Ca obtained for DS of K-Inc record had a slope of 0.27 (Fig. 4A), pointing out that the stalagmite failed to reproduce the thermodynamics precepts of PCP for ln(Mg/Ca) vs. ln(Sr/Ca) (Sinclair, 2011). The inconsistency in the Mg/Ca response throughout the entire record of K-Inc made us summarily discard Mg/Ca from paleoclimatic interpretations. In turn, the plot of the molar ratios of K-Inc record in the ln-space of Sr/Ca and Ba/Ca following the correlation

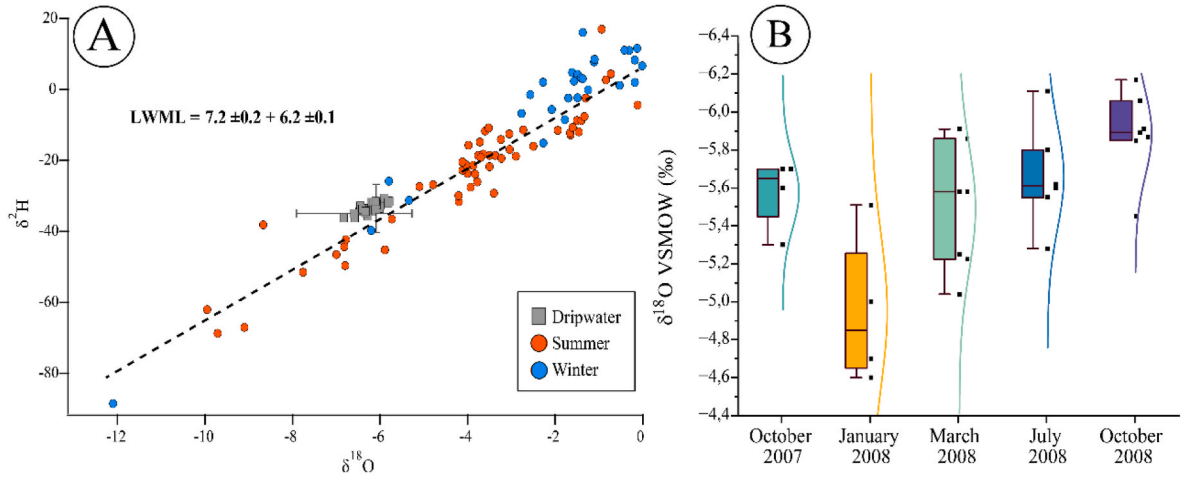

Fig. 3. (A) Composition $\delta^{2}H$ vs. $\delta^{18}O$ for rainwater collected from 1962 to 1984 at the meteorological station of Veracruz database from GNIP-IAEA; summer rainfall (orange dots), winter rainfall (blue), and the dripwater from Karmidas (gray squares). Error bars correspond to the amount-weighted $\delta^{18}O$ and $\delta^{2}H$ for the Veracruz rainfall samples. Local Meteoric Water Line (black) is also presented. (B) Whisker plot (solid: amount-weighted $\delta^{18}O$ average, line = average, box: ± 1SD, whisker = max and min) showing the progression of $\delta^{18}O$ values from drip water collected in 5 sites at Karmidas cave during 2007–2008.

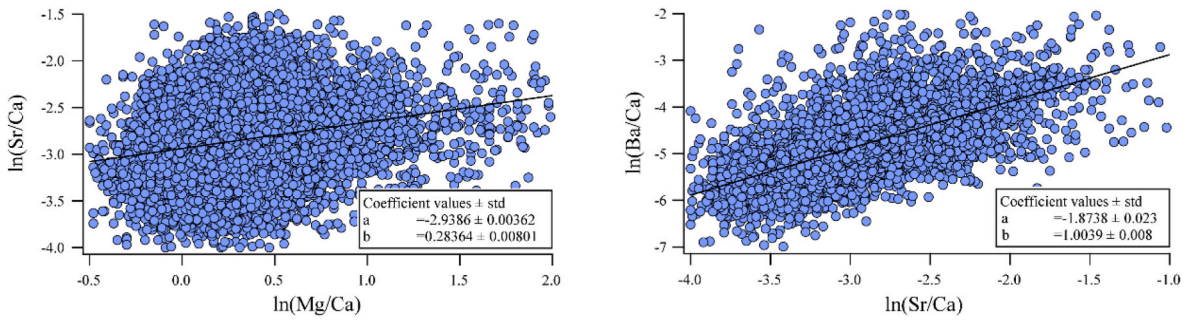

Fig. 4. Tests for PCP: (A) ln(Mg/Ca) vs. ln(Sr/Ca) following Sinclair (2011); (B) ln(Sr/Ca) vs. ln(Ba/Ca) following Bernal et al. (2016). The black lines correspond to the slope uncertainty. The slope of ln(Mg/Ca) vs. ln(Sr/Ca) plot does not follow thermodynamic precepts for PCP (0.88 ± 0.13), while the ln(Sr/Ca) vs. ln(Ba/Ca) co-vary linearly with a slope of 1.02 ± 0.08, revealing the occurrence of PCP.

with a slope of 1.02 ± 0.08 (Fig. 4B), which is another way of revealing the occurrence of PCP due to the seasonally sensitive of DS to the CO_2 degassing according to Bernal et al. (2016). Therefore, K-Inc followed the PCP requirements for ln(Sr/Ca) vs. ln(Ba/Ca), enabling the use of the high-resolution trace element ratios as a proxy to infer drier periods.

The trace element record for the whole stalagmite comprised more than 18600 points and was smoothed using a moving average with a binomial window. We stacked the data using the youngest age point derived from U/Th, estimated at 264 ± 12 years, at 19 mm. Smoothing with 15 points per year for Sr/Ca resulted in 267 cycles, achieving cyclicity close to annual resolution. Similarly, smoothing Ba/Ca with 17 points per cycle also resulted in 267 cycles. We will elaborate further on our paleoclimatic interpretations based on this smoothed dataset.

We compared the smoothed Sr/Ca data with three databases (Fig. 5): the average regional meteorological data series, data from the Climate Hazards Group InfraRed Precipitation (CHIRPS), and the Global Precipitation Climatology Centre (GPCC). For CHIRPS and GPCC, we extracted data from the quadrant spanning 20°N to 20°25′N and 97°.5′W to 97.75°'W. The trend of the precipitation data compared to the Sr/Ca ratio indicates a synchronous response of the PCP over time.

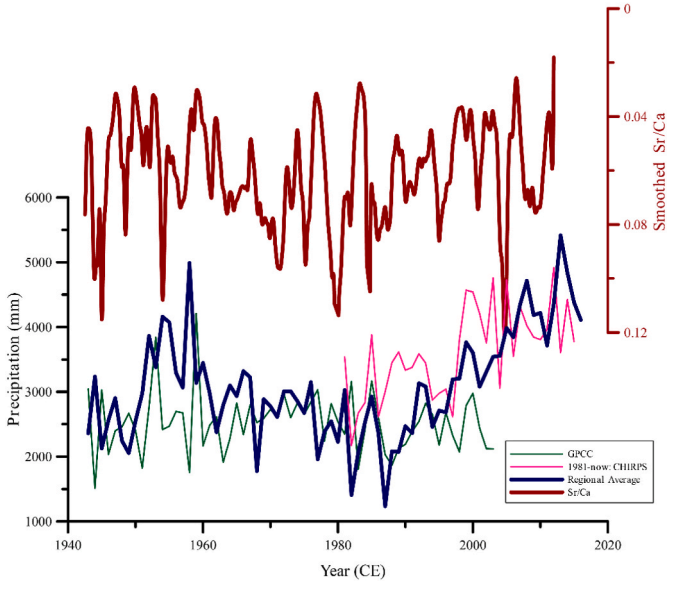

Fig. 5. The smoothed Sr/Ca ratio (dark red line) is compared with the average regional meteorological data series from the cities of Zapotitlan de Méndez, Cutzalán del Progreso, and Xicotepec de Juarez (dark blue line). Additionally, the Climate Hazards Group InfraRed Precipitation with Station data (CHIRPS), a quasi-global rainfall dataset from 1981 to the present, is represented by the pink line, and the Global Precipitation Climatology Centre (GPCC), which offers gridded gauge-analysis products based on quality-controlled station data, is shown by the green line.

5. Discussions

5.1. The limitations in assessing the use of oxygen isotopes as a result of different sources

The observed behavior of the oxygen isotopic composition during monitoring rainwater, dripping water, and neoformed calcite drives our reasoning. The competence of neoformed calcite to preserve the isotopic composition of both frontal and convective rain highlights crucial points for consideration. Firstly, the cave's location extends beyond the exclusive influence of tropical regions and the straightforward association of the isotopic signal with the amount effect; thus, inferring the local hydroclimate based on $\delta^{18}O$ data is not so intuitive. Secondly, the isotopic record may indicate periods of atmospheric reorganization that are more influenced by frontal rains rather than convective precipitation or vice versa. Nevertheless, the establishment of these moments of atmospheric reorganization in the geological past is intricate due to the time scale of events.

The Atlantic Meridional Variability (AMV) index is defined by the mean SST of the North Atlantic basin (0°–70°N, 80°W–0°). Cold (Warm) AMV conditions are ascribed to atmospheric patterns that trigger phases of intense (reduced) basin-wide winds that drive enhanced (shallow) thermal gradient between two atmospheric pressure zones known as the NASH of Azores (38°N) and the Arctic polar low pressure of Iceland (60°N). The preview mentioned conditions are the precursor to the positive (negative) NAO mode, when the circulation of the intergyre becomes anticyclonic (cyclonic), strengthening (reducing) westerlies, intensifying (weakening) the thermohaline circulation and enhancing (diminishing) northward heat transport, boosting (impairing) the redistribution of sea surface energy to high levels of the atmosphere (Knight et al., 2005; Grossmann and Klotzbach, 2009). The conjunction between AMV and NAO is a critical large-scale teleconnection that has a plethora of secondary effects on the climate system of North America, such as increasing cold fronts under the negative NAO phase generating frontal rainfall over Texas during the boreal winter (Hardy and Henderson, 2003).The global climate during the Little Ice Age (LIA), from 1450 to 1850 CE, experienced three grand solar minima (the Spörer, Maunder, and Dalton Minima). These periods coincided with Gleissberg 88-year solar cycle (Gleissberg, 1958; Peristykh and Damon, 2003), marked by significant changes in the variability of Arctic sea-ice cover, and drove the global climate patterns. The observed in-phase relationship between the high-resolution $\delta^{18}O$ data from the K-Inc stalagmite and the temporal patterns in Arctic ice volume (Fig. 6A and B), along with the negative correlation ($r = -0.43$) between ice extension and $\delta^{18}O$ values, indicates a significant impact on modulating moisture sources.

The spatial variations in atmospheric $\delta^{18}O$ are nearly ten times greater than those observed in the ocean (Lachniet, 2009). This makes

the link between extratropical atmospheric features and our $\delta^{18}O$ data especially relevant during the LIA. While the NAO reconstruction by Ortega et al. (2015) suggests a predominantly negative phase from 1600 to 1850 CE, the lack of high-resolution $\delta^{18}O$ records in Mexico hinders our ability to interpret this signal. Currently, no stalagmite $\delta^{18}O$ records from Mexico have the temporal resolution needed to capture seasonal changes. As a result, directly correlating NAO reconstructions with stalagmite records in the region is not feasible. This gap highlights the need for future studies to obtain higher-resolution $\delta^{18}O$ data to improve our understanding of past climate variability in Mexico.

The K-Inc $\delta^{18}O$ record shows a significant correlation with AMV, with a correlation coefficient of r = 0.5 and a response lag of about 20 years (Supplementary Fig. 2). Geological records from the Gulf of Mexico, such as those reported by Thirumalai et al. (2018), indicate below-average sea surface temperatures (SST) during the LIA, with the lowest values between 1600 and 1800 CE. Our findings suggest that this period is crucial for interpreting $\delta^{18}O$ data. Relying solely on the amount effect to understand regional hydroclimate may be inadequate, as multiple climatic factors could obscure the influence of precipitation on $\delta^{18}O$ values. This calls for a more nuanced interpretation of $\delta^{18}O$ records, considering additional factors beyond the amount effect.

We compared the $\delta^{18}O$ records from Karmidas Cave with those from Aljojuca Maar Lake (Bhattacharya et al., 2015), Bonita Cave (23°N, 99°W; Wright et al., 2022), and Tzabnah Cave (20.73°N 89°47W; Medina-Elizalde et al., 2010). The correlation between $\delta^{18}O$ records from K-Inc and Aljojuca Maar Lake matched well during the LIA (r = 0.40) but showed a time lag (Fig. 6E). Despite the good visual alignment between the records, a hastier analysis may imply an incongruous signal of regional precipitation. Correlations with Bonita Cave (r = 0.18) and Tzabnah Cave (r = −0.10) were weak, showing limited consistency (Fig. 6F and G). Although Karmidas Cave is influenced by different climatic and hydrological sources, the lack of monitoring and understanding of other caves makes it difficult to interpret Mexican climate dynamics. Our study emphasizes the need for site-specific monitoring to assess regional climate better. Without such monitoring, interpreting paleoclimate records from Karmidas Cave and applying them to broader Mexican climate studies remains challenging.

In contrast, the $\delta^{18}O$ record from a stalagmite in Juxtlahuaca Cave in western Mexico shows an antiphase with the $\delta^{18}O$ values from Karmidas Cave. This comparison suggests an apparent polarity between Mexico's western and eastern regions, likely due to different atmospheric forces and the influence of the Pacific Ocean on the Juxtlahuaca Cave stalagmite (Fig. 6H). In fact, Lachniet et al. (2017) noted slight differences in hydrological patterns between Mexico's eastern and western regions during the current rainy season. However, the low correlation (r = 0.06) suggests uncorrelated events. Further studies are needed to explore this issue, particularly with higher resolution and trace element ratios from Juxtlahuaca Cave. In the next section, we will examine the trace element ratios of the K-Inc stalagmite to assess regional hydrological settings, water retention, and infiltration dynamics in the epikarst at a higher resolution.

5.2. *Trace element ratios revealing the pacing of ENSO over eastern Mexico during LIA*

We have noted a distinct pattern in the Sr and Ba to Ca ratios within the K-Inc stalagmite compared to the oxygen isotopic measurements, with $\delta^{18}O$ being related to atmospheric variability and trace element ratios with the infiltration in the epikarst. Recognizing that Sr/Ca and Ba/Ca fluctuations are inversely correlated with water availability within the epikarst and its association with seasonal contrast patterns makes it imperative to investigate climatic events characterized by shorter periodicity.

During the cold phase of AMV, the climatological position of the Intertropical Convergence Zone (ITCZ) is displaced to the South Hemisphere toward the hemisphere with warmer SST (Rind, 1998). The ITCZ

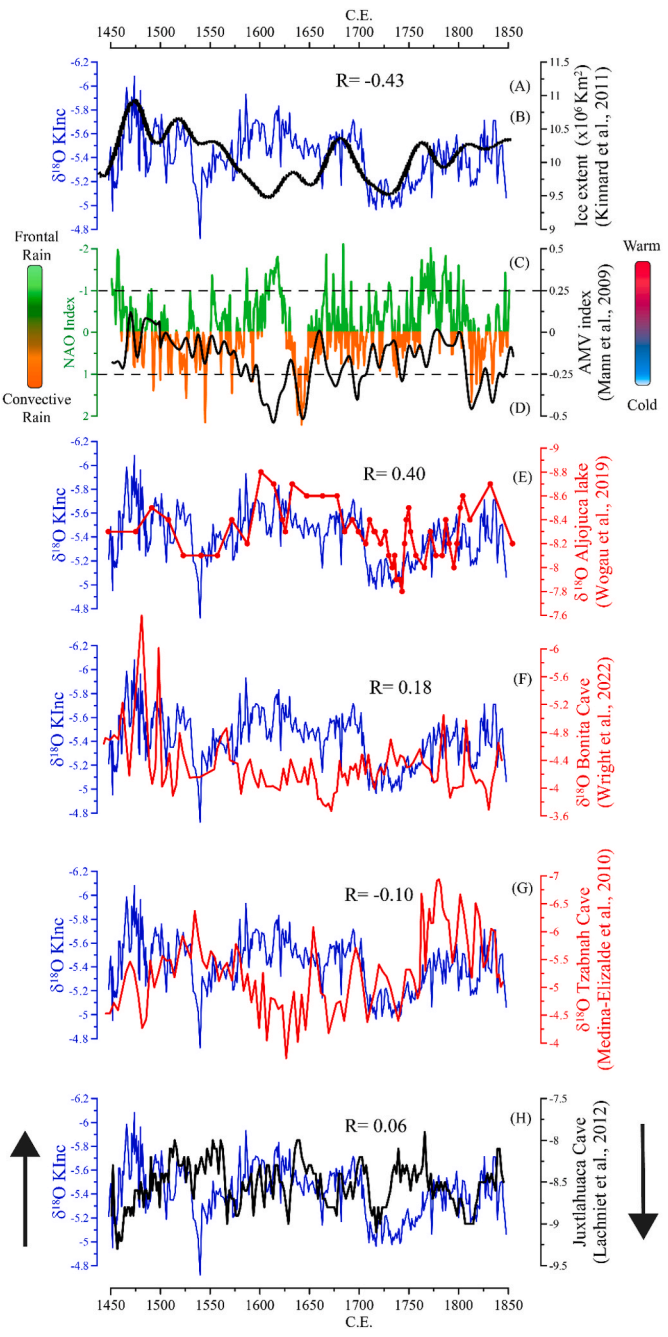

Fig. 6. (A) $\delta^{18}O$ from K-Inc (in blue), this study; (B) Arctic ice extent (Kinnard et al., 2011), note that the Y axis is inverted; (C) Atlantic Meridional Variability (AMV), in black (Mann et al., 2009); (D) North Atlantic Oscillation (NAO) index (Ortega et al., 2015). (E) $\delta^{18}O$ from Aljojuca Lake (Wogau et al., 2019); (F) Bonita cave (Wright et al., 2022); (G) Tzabnah cave (Medina-Elizalde et al., 2010); (H) $\delta^{18}O$ from Juxtlahuaca Cave (Lachniet et al., 2012). Note for all stalagmite plots except this one Y axis is inverted. More negative $\delta^{18}O$ values indicate a more significant amount of convective rain.

is a strong rainfall band formed by the convergence of the northern and southern trade winds near the equator. A composite of proxies related to the core occurrence of ITCZ indicated that it was spread to the Southern Hemisphere during most of the LIA, particularly during 1600–1800 CE (Lechleitner et al., 2017, Fig. 7A). When the ITCZ reaches its southmost position, the equatorial trade winds deplete, causing the recession of the cold tongue at the eastern equatorial Pacific (EEP) and leading to the onset of the warm mode of ENSO (El Niño) (Atwood and Sachs, 2014).

The Caribbean Low-Level Jet (CLLJ) exhibits a positive correlation

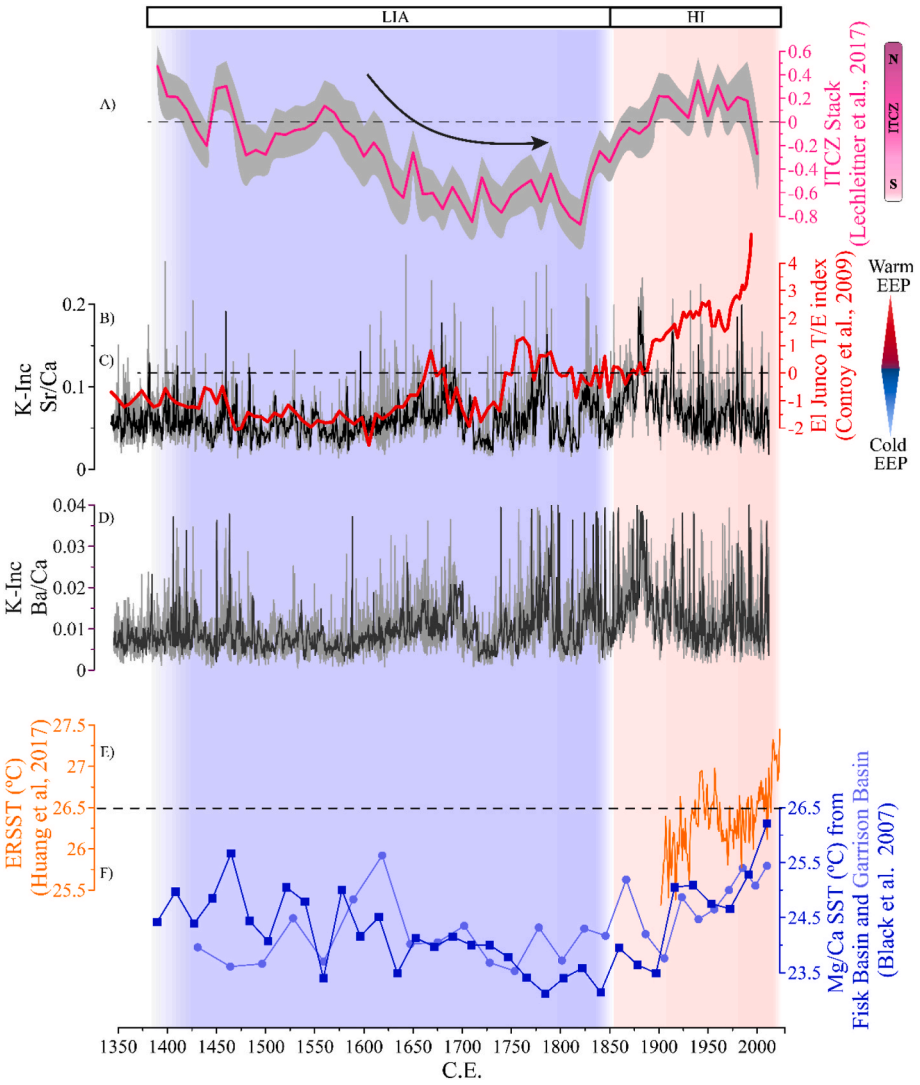

Fig. 7. (A) Intertropical Convergence Zone (ITCZ) stack (Lechleitner et al., 2017); (B) El Junco T/E index (Conroy et al., 2009); (C) Sr/Ca (mmol/mol; this study), with a smooth of 15 points; (D) Ba/Ca (mmol/mol; this study), with a smooth of 16 points; (E) NOAA Extended Reconstructed Sea Surface Temperature (ERSST) (Huang et al., 2017); (F) Geological SST records from the Gulf of Mexico based on Mg/Ca (Black et al., 2007). The light blue background indicates the Little Ice Age period (LIA), and the light red background indicates the Historical Interval (HI). The Trace elements of K-Inc indicate that the vicinities of Zapotitlán de Méndes were not particularly dry during the LIA time interval, except for punctual and prolonged warm zonal events in the eastern equatorial Pacific (EEP). In contrast, the warm zonal events in EPP do not imply dry conditions during the HI period.

with the meridional wind anomalies at the 925-hPa level. The latter transports moisture from the ocean to the central United States via the Gulf of Mexico. There is a congruence between a slackened North Atlantic subtropical high of Azores (NASH) during the cold phase of AMV and enhanced relevance of the meridional wind anomalies at the 925-hPa level intrusion along Mexico's east coast (Giannini et al., 2001; Wang, 2007).

Several indices monitor the tropical Pacific, all based on SST anomalies in specific regions. The index EN1+2 (0–10°S, 90-80°W) is related to the position of San Cristóbal Island. El Junco Lake is placed on San Cristóbal Island, Galápagos (1°S, 89°W), and it is highly responsive to SST zonal variability, analogous to ENSO events. Conroy et al. (2009) built an index of the ratio of tychoplanktonic to epiphytic diatoms (T/E), ascribing the increase of El Junco Lake level to high values of the index because of enhanced precipitation during warmer Galapagos SST. Cold ENSO-dominated conditions prevailed during the LIA(Yan et al., 2011; Falster et al., 2023), and the harmonic response between the increase of the T/E index from El Junco Lake and the values of Sr and Ba to Ca ratios from K-Inc during LIA (r = 0.36; Fig. 8B) endorses the relationship between warm zonal SST in EEP and mild meridional wind anomalies at the 925-hPa level, with significant reductions in moisture flux into northeastern Mexico (Fig. 7B, C, and 7D).

Current meteorology studies relate warm ENSO to dryer summers in the eastern portion of the Mexican territory due to the eastward displacement of the Walker cell, postponing the formation of clouds and precipitation (Bravo-Cabrera et al., 2017), as well as lowering the northeast trade winds and the efficiency of moister transport toward the land. Our interpretation suggests that the pace of warm SST zonal events in EEP did not necessarily generate an arid condition in the region of Karmidas due to the increased frequency of frontal rains, but we suggest an enhanced seasonal contrast. Consequently, decreasing the water infiltration in the epikarst increased the effect of PCP reflected in the high ratios of Sr/Ca and Ba/Ca from K-Inc (Fig. 8B, C, and 8D).

Our proxies bind the warm SST zonal phases in EEP (EN1+2) to a prolonged shortage of rain in northeastern Mexico whilst associating cold SST zonal phases in EEP with a more constant influx of moisture in the same areas. The occurrence of frontal rain is provided by stronger meridional wind anomalies at the 925-hPa level, derived from the cold

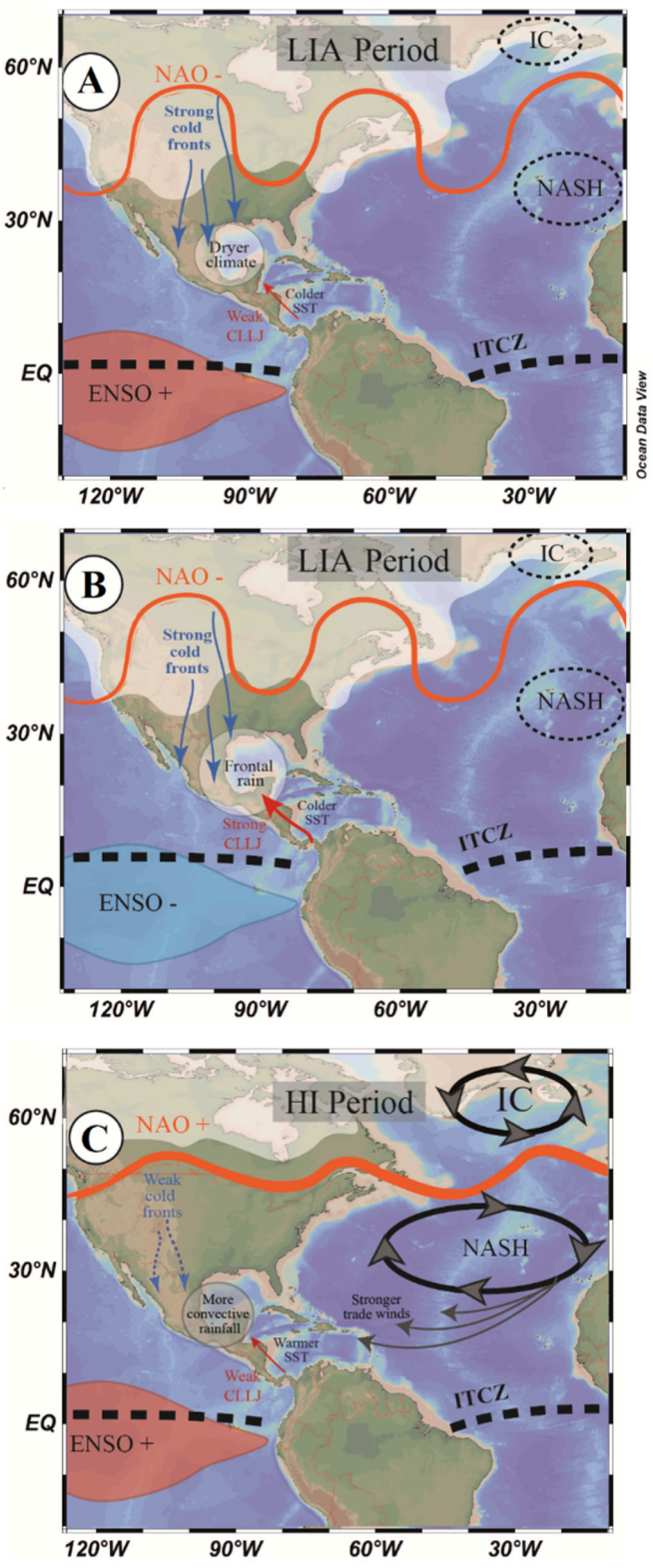

Fig. 8. Conceptual model of the three climate scenarios proposed throughout the manuscript. Moreover, the (A) and (B) are temporally located in the LIA interval, when the North Atlantic Subtropical High (NASH) was weak, and the North Atlantic Oscillation (NAO) was predominantly negative. These differ in the predominance of warm and cold ENSO events and the intrusion of moist-laden air from 950 hPa anomalies driving the path of the Caribbean low-level jets (CLLJ), with scenario (B) more conducive to forming frontal rain over eastern México. The climate scenario (C) represents the Historical Interval (HI) from 1850 CE onwards. Although warm ENSO is predominant during HI, a stronger NASH generates a positive NAO, fewer cold surges, and stronger Trade winds; the global warmer sea surface temperature and greater solar irradiance are boundary conditions that enable the predominance of convective rain in eastern México.

zonal SST in EEP, which fosters the encounter of moisture-laden intrusions with the increased frequency of cold surges during boreal winter, propelled by the dominant negative NAO-like phase. During the LIA, the SST in the Gulf of Mexico was below the average of HI SST (8F), reducing moisture convection to the atmospheric boundary layer (Graham and Barnett, 1987). This climate scenario attributes greater relevance to frontal rain over eastern Mexico for the LIA.

5.3. The Historical Interval

Severe drought conditions preceded the Mexican Revolution (November 1910) (Lachniet et al., 2012, 2017; Stahle et al., 2016), and it is known that the Karmidas Cave artificial aperture was officially dated 1917–1919 CE on the grounds of finding water to maintain the planting of sugar cane and corn near the cave. The dryer conditions were operating and possibly prompted the locals to look for water sources inside the Karmidas Cave, as indicated by the substantial increase in Sr/Ca and Ba/Ca of both stalagmites from ~1850 to ~1900. A dryer climate scenario tends to strengthen CO_2-degassing in ventilated caves, enhancing the effect of PCP and enriching the $\delta^{18}O$ records. Based on the Hendy test (Supplementary Fig. 1), we suggest that increased cave ventilation, closely related to the artificial cave opening, resulted in the 20-year oscillation observed in $\delta^{18}O$ measurements from 1900 CE onwards, biasing the $\delta^{18}O$ climate-related information. Notwithstanding, the decrease in Sr/Ca and Ba/Ca ratios against the pace of warm SST zonal events in EEP ($r = -0.2$; Sr/Ca) caught our attention (Fig. 7B). Our proxies indicate wetter climate conditions for HI than LIA, and this circumstance may be justified if warm SST zonal events in EEP have lost relevance for the regional hydroclimate during the HI (Fig. 8B, C, 8D). Thus, the climate background of the HI deserves further investigation despite the potential anthropogenic meddling on the $\delta^{18}O$ record post-1900 CE.

Here, we need to punctuate that the average global SST warmed up over the last century, and the Gulf of Mexico records do not diverge from this pattern (8E and 8F) (Richey et al., 2009; DeLong et al., 2014; Thirumalai et al., 2018). The SST significantly influences the distribution and transport of heat and moisture, altering precipitation and air temperature modes and intensifying its impact on local climate (Graham and Barnett, 1987). Bishop et al. (2018) used the National Center for Environmental Prediction (NCEP) and National Center for Atmospheric Research (NCAR) Reanalysis (NCEP-NCAR) data (Kalnay et al., 1996) from 1948 to 2005. They observed the southward shift or expansion in the western ridge of the fall NASH from its climatological mean. The results from Bishop et al. (2018) also support SST-forced simulations for the Caribbean region, indicating the strengthening of NASH and its westward displacement (Li et al., 2011, 2012), which intensifies the trade winds carrying high moisture levels into the windward side of the Sierra Madre Oriental. Comparing the relationship between ENSO and NASH, Li et al. (2013) concluded that the influence of NASH might be more decisive in SE US summer precipitation from 1948 to 2007. These studies indicate that NASH gained strength during the HI, dwindling the relevance of ENSO for eastern Mexico, and justify our findings.

Since the LIA, solar irradiance has increased, causing the waters of the Gulf of Mexico to absorb more heat through insolation and retain a more significant amount of this heat. By winter, the continent becomes cooler than the nearby sea, intensifying westward winds that draw out warmth and moisture from the Gulf of Mexico (Gutierrez de Velasco and Winant, 1996; Chang and Oey, 2010). The higher solar irradiance and warmer SST at the Gulf of Mexico might have reinforced the land-sea thermal contrast, enhancing the efficiency of moisture transport along the east of Mexico during the HI compared to LIA, also fortified by the westward NASH. Wright et al. (2022) highlighted the relevance of SST for the regional hydroclimate at the Bonita Cave record during the HI, and our results confirm their inferences due to the response of the trace elements ratios (Sr/Ca and Ba/Ca) of K-Inc. In short, despite the $\delta^{18}O$ record of K-Inc being biased by local human influence over the HI due to the artificial cave opening, the trace elements of K-Inc can still provide valuable information on the hydroclimatic conditions.

6. Conclusions

We produced multi-proxies records from the stalagmite Karmidas-inclined (K-Inc). We compared them with records from independent proxies, providing information on the past hydroclimate in the central east of México during the last ~600 years, covering the Little Ice Age (LIA) and the Historical Interval (HI). The $\delta^{18}O$ signal of K-Inc monitoring of the Karmidas cave points to a region with a lot of precipitation throughout the year. The K-Inc drip point preserved seasonal variability, with the influence of frontal rains during the winter and the amount effect during the summer. The record of K-Inc is under the pacing of Artic Ice volume during the LIA. The resolution of the $\delta^{18}O$ data was unable to identify the NAO frequency, still we suggest the influence of the negative phase of the North Atlantic Oscillation (NAO) played a significant role by propitiating the occurrence of cold surges. Therefore, it would not be an ideal record to elucidate the hydroclimate through the amount effect.

Nevertheless, the weakened North Atlantic Subtropical High (NASH) has emerged as a crucial ocean-atmospheric feature that influences the interaction of meridional low-level jets in northern tropical latitudes. This includes cold surges resulting from negative NAO-like state and a strong Caribbean Low-Level Jet (CLLJ), the latter driven by cold SST zonal equatorial eastern Pacific (EEP) events. The response of the trace species (Sr/Ca and Ba/Ca) from a stalagmite K-Inc revealed a momentary shift in the seasonal extension during LIA, with the vicinity of Karmidas Cave becoming drier during warm SST zonal events in EEP. A weakened NASH provided more relevance to the EEP SST zonal variability during LIA than the HI. We elaborated a conceptual model with the main climate features of each proposed scenario (Fig. 8A and B).

During the HI, we noticed a prominent coupling between the higher Sr and Ba to Ca ratios of K-Inc and the pace of warm SST zonal mode in EEP. In contrast to the LIA, three parameters have significantly contributed to the enhanced advection of moisture into the eastern coast of Mexico during the HI: 1- The warmer SST at the Gulf of Mexico; 2- More intense trade winds due to a strengthened NASH; and 3- The increase of solar irradiance, enhancing the thermal contrast between inland areas and the adjacent ocean during the winter (Fig. 8C). All these parameters work in tandem, strengthening the precipitation regime in eastern Mexico and demonstrating that the zonal EEP variability became less relevant over the HI, bringing light to the functioning of the main climatic drivers that played a more significant role over each climatic condition.

Statement

During the preparation of this work, the author(s) used Grammarly in order to improve the english writing. After using this tool/service, the author(s) reviewed and edited the content as needed and take(s) full responsibility for the content of the publication.

Authors contribution

All authors made substantial contributions to this submission.

- Patricia Piacsek, Ph.D. Manuscript writing, data analysis, laboratory processes (LAICP-MS and isotopes carbonate samples), and participation in field trips to the Karmidas cave.
- Juan Pablo Bernal, Ph.D. Research financer, assistance in the design of the manuscript, participation in field trips to the Karmidas cave.
- María del Pilar Aliaga-Campuzano, Master Degree. Participated in field trips to the Karmidas cave and collected cave monitoring data.
- Luis Bernardo Chavero, Master Degree. Data analysis and participation in field trips to the Karmidas cave. Cover Letter

•Fernanda Lases-Hernández, Ph.D. Laboratory processes (Isotopes in water samples) and manuscript editing.
•Francisco William da Cruz, Ph.D. Laboratory processes (isotope carbonate samples) and manuscript editing.
•Nicolás Misailidis Strikís, Ph.D. Manuscript editing and data analysis.
•Marília Harumi Shimizu, Ph.D. Manuscript editing and data analysis.
•Liliana Corona-Martinez, Master Degree. Laboratory processes (U-Th dating), manuscript editing, and participation in field trips to the Karmidas cave.
•Veronica M. Ramirez, Ph.D. Laboratory processes (isotope carbonate samples).
•Herminio Rojas. Owner and responsible for maintaining the Karmidas cave, providing assistance for field trips, and collecting cave monitoring data.

Declaration of competing interest

The authors declare that they have no known competing financial interests or personal relationships that could have appeared to influence the work reported in this paper.

Data availability

Data will be made available on request.

Acknowledgments

Funding for this work was provided by PAPIIT – UNAM grant number IG100722. This work was supported by the UNAM Postdoctoral Program (POSDOC) to Patricia Piacsek. This study was financed by the FAPESP 2022/08359-7 grant to F. W. Cruz. This study was financed by the grant ERC project LAST JOURNEY (ERC_Adv_834514) to V. M. Ramirez. This study was financed in part by the São Paulo Research Foundation - FAPESP (grant numbers: 2022/08359-7) to NM Strikis, Rio de Janeiro Research Foundation – FAPERJ (grants E-26-201.421-2021 and E-26211.352-2021) to N.M.S. and Conselho Nacional de Desenvolvimento Científico e Tecnológico - CNPq (grant 312343/2022-1) to N.M. Strikis. We thank Carlos Ortega Bregon for his technical support with the LA-ICP-MS and Ofelia Pérerz Arvízu at the Laboratorio de Estudios Isotópicos (LEI) and Carolina Muñoz Torres, all at the Instituto de Geociências de Juriquilla. We thank technical support to Jessica Olivares Amador and Korynthia López Aguiar. We are grateful to the team of the Laboratório Isótopos Estáveis at the Department of Sedimentary and Environmental Geology (GSA) of the University of São Paulo for helping with isotope measurements in the speleothem. We acknowledge the data repositories of Past Global Changes (PAGES), the National Oceanic and Atmospheric Administration (NOAA), the International Atomic Energy Agency (GNIP - IAEA), and original data generators that enable the scientific community to enhance their discussions. I would like to thank the JQSR reviewers for all their guidance and improvements to the paper. Lastly, I dedicate this work to the memorium of my dearest friend, Beatriz Keiko Naruto.

Appendix A. Supplementary data

Supplementary data to this article can be found online at https://doi.org/10.1016/j.quascirev.2024.108981.

References

Aliaga-Campuzano, M.P., López-Martínez, R., Dávila-Harris, P., et al., 2017. Timing of speleogenesis of Las Karmidas Cave (Mexico): first description of pseudokarst developed in ignimbrite. Int. J. Speleol. 46, 331–343. https://doi.org/10.5038/1827-806X.46.3.2097.

Atwood, A.R., Sachs, J.P., 2014. Separating ITCZ-and ENSO-related rainfall changes in the Galápagos over the last 3 kyr using D/H ratios of multiple lipid biomarkers. Earth Planet Sci. Lett. 404, 408–419. https://doi.org/10.1016/j.epsl.2014.07.038.

Belt, B.C., 1925. Stratigraphy of the tampico district of Mexico. American Association of Petroleum Geologists 9 (1), 136–144.

Bernal, J.P., Cruz, F.W., Stríkis, N.M., et al., 2016. High-resolution holocene south American monsoon history recorded by a speleothem from botuverá cave, Brazil. Earth Planet Sci. Lett. 450, 186–196. https://doi.org/10.1016/j.epsl.2016.06.008. ISSN 0012-821X.

Bhattacharya, T., Coats, S., 2020. Atlantic-pacific gradients drive last millennium hydroclimate variability in Mesoamerica. Geophys. Res. Lett. 47 (13), e2020GL088061. https://doi.org/10.1029/2020GL088061.

Bhattacharya, T., Byrne, R., Böhnel, H., et al., 2015. Cultural implications of late Holocene climate change in the Cuenca Oriental, Mexico. Proc. Natl. Acad. Sci. USA 112 (6), 1693–1698. https://doi.org/10.1073/pnas.1405653112.

Bishop, D.A., Williams, A.P., Seager, R., et al., 2018. Investigating the causes of increased 20th-century fall precipitation over the southeastern United States. J. Clim. 32 (2), 575–590. https://doi.org/10.1175/JCLI-D-18-0244.1.

Black, D.E., Abahazi, M.A., Thunell, R.C., Kaplan, A., Tappa, E.J., Peterson, L.C., 2007. An 8-century tropical Atlantic SST record from the Cariaco Basin: baseline variability, twentieth-century warming, and Atlantic hurricane frequency. Paleoceanography 22, PA4204. https://doi.org/10.1029/2007PA001427.

Bravo-Cabrera, J.L., Azpra, E., Zarraluqui, V., et al., 2017. Effects of El Niño in Mexico during rainy and dry seasons, an extended treatment. Atmósfera 30 (3), 221–232. https://doi.org/10.20937/ATM.2017.30.03.03.

Carrasco-Núñez, G., Bernal, J.P., Dávila, P., et al., 2018. Reappraisal of Los Humeros volcanic complex by new U/Th zircon and $^{40}Ar/^{39}Ar$ dating: implications for greater geothermal potential. G-cubed 19, 132–149. https://doi.org/10.1002/2017GC007044.

Cervantes-Zamora, Y., Cornejo-Olguín, S.L., Lucero-Márquez, R., Espinoza-Rodríguez, J. M., Miranda-Vázquez, E., Pine-da-Velázquez, A., 1990. Provincias Fisiográficas de México, Clasificación de Regiones Naturales de México II, IV. 10.2, Atlas Nacional de México. Vol. II, scale 1:4000000. México. Instituto de Geografía. Universidad Nacional Autónoma de México.

Chang, Y., Oey, L., 2010. Eddy and wind-forced heat transports in the Gulf of Mexico. J. Phys. Oceanogr. 40, 2728–2742. https://doi.org/10.1175/2010JPO4474.1.

Cheng, H., Lawrence, E.R., Shen, C.-C., et al., 2013. Improvements in 230Th dating, 230Th and 234U half-life values, and U–Th isotopic measurements by multi-collector inductively coupled plasma mass spectrometry. Earth Planet Sci. Lett. 371–372, 82–91. https://doi.org/10.1016/j.epsl.2013.04.006. ISSN 0012-821X.

Conroy, J.L., Overpeck, J.T., Cole, J.E., et al., 2009. Variable oceanic influences on western North American drought over the last 1200 years. Geophys. Res. Lett. 36 (17), L17703–L17709. https://doi.org/10.1029/2009GL039558. ISSN 0094-8276.

Coplen, T.B., 1996. New guidelines for reporting stable hydrogen, carbon, and oxygen isotope-ratio data. Geochem. Cosmochim. Acta 60 (17), 3359–3360. https://doi.org/10.1016/0016-7037(96)00263-3.

Cruz, F.W., Burns, S.J., Jercinovic, M., et al., 2007. Evidence of rainfall variations in Southern Brazil from trace element ratios (Mg/Ca and Sr/Ca) in a Late Pleistocene stalagmite. Geochem. Cosmochim. Acta 71 (9), 2250–2263. https://doi.org/10.1016/j.gca.2007.02.005. ISSN 0016-7037.

Cuna, E., Zawisza, E., Caballero, M., et al., 2014. Environmental impacts of Little Ice Age cooling in central Mexico recorded in the sediments of a tropical alpine lake. J. Paleolimnol. 51, 1–14. https://doi.org/10.1007/s10933-013-9748-0.

Day, C.C., Henderson, G.M., 2013. Controls on trace-element partitioning in cave-analogue calcite. Geochem. Cosmochim. Acta 120, 612–627. https://doi.org/10.1016/j.gca.2013.05.044. ISSN 0016-7037.

de Villiers, S., Greaves, M., Elderfield, H., 2002. An intensity ratio calibration method for the accurate determination of Mg/Ca and Sr/Ca of marine carbonates by ICP-AES. G-cubed 3 (1). https://doi.org/10.1029/2001GC000169.

DeLong, K.L., Flannery, J.A., Poore, R.Z., Quinn, T.M., Maupin, C.R., Lin, K., Shen, C.C., 2014. A reconstruction of sea surface temperature variability in the southeastern Gulf of Mexico from 1734 to 2008 CE using cross-dated Sr/Ca records from the coral Siderastrea siderea. Paleoceanography 29 (5), 403–422.

Falster, G., Konecky, B., Coats, S., et al., 2023. Forced changes in the Pacific Walker circulation over the past millennium. Nature 622, 93–100. https://doi.org/10.1038/s41586-023-06447-0.

Giannini, A., Cane, M.A., Kushnir, Y., 2001. Interdecadal changes in the ENSO teleconnection to the caribbean region and the North Atlantic oscillation. J. Climate 14, 2867–2879. https://doi.org/10.1175/1520-0442(2001)014<2867:ICITET>2.0.CO;2.

Gleissberg, W., 1958. The eighty-year sunspot cycle. J. Br. Astron. Assoc. 68, 148–152.

Graham, N., Barnett, T.P., 1987. Observations of sea surface temperature and convection over tropical oceans. Science 238, 657–659.

Grossmann, I., Klotzbach, P.J., 2009. A review of North Atlantic modes of natural variability and their driving mechanisms. Journal of Geophysical Research: Atmospheres 114 (D24), D24107. https://doi.org/10.1029/2009JD012728.

Gutierrez de Velasco, G.G., Winant, C.D., 1996. Seasonal patterns of wind stress and wind stress curl over the Gulf of Mexico. J. Geophys. Res. 101 (C8), 18127–18140. https://doi.org/10.1029/96JC01442.

Hardy, J.W., Henderson, K.G., 2003. Cold front variability in the southern United States and the influence of atmospheric teleconnection patterns. Phys. Geogr. 24 (2), 120–137. https://doi.org/10.2747/0272-3646.24.2.120.

Heim, A., 1926. Notes on the jurassic of tamazunchale (Sierra Madre oriental, México). Eclogae Geol. Helv. 20 (1), 82–89.

Hernández-Mendiola, E., Bernal, J.P., Lounejeva, E., et al., 2011. U-series dating of carbonates using inductively coupled plasma-quadrupole mass spectrometry. Quat.

Geochronol. 6 (6), 564–573. https://doi.org/10.1016/j.quageo.2011.09.001. ISSN 1871-1014.
Huang, et al., 2017. Extended reconstructed Sea Surface temperatures version 5 (ERSSTv5): upgrades, validations, and intercomparisons. J. Clim. https://doi.org/10.1175/JCLI-D-16-0836.1.
Instituto Nacional de Geografía y Estadística, INEGI, 2020. Resultados del Censo Nacional de Población y Vivienda. Disponible en: Disponible en. https://www.inegi.org.mx/programas/ccpv/2020/.
Jaffey, A.H., Flynn, K.F., Glendenin, L.E., et al., 1971. Precision measurement of half-lives and specific activities of 235U and 238U. Phys. Rev. C 4 (5), 1889.
Kalnay, K.E., Kanamitsu, M., Kistler, R., et al., 1996. The NCEP/NCAR 40-year Reanalysis project. Bull. Am. Meteorol. Soc. 77, 437–472. https://doi.org/10.1175/1520-0477(1996)077<0437:TNYRP>2.0.CO;2.
Kim, S., O'Neil, J.R., 1997. Equilibrium and nonequilibrium oxygen isotope effects in synthetic carbonates. Geochem. Cosmochim. Acta. ISSN: 0016-7037 61 (16), 3461–3475. https://doi.org/10.1016/S0016-7037(97)00169-5.
Kinnard, C., Zdanowicz, C., Fisher, D., et al., 2011. Reconstructed changes in Arctic sea ice over the past 1,450 years. Nature 479, 509–512. https://doi.org/10.1038/nature10581.
Knight, J.R., Allan, R.J., Folland, C.K., Vellinga, M., Mann, M.E., 2005. A signature of persistent natural thermohaline circulation cycles in observed climate. Geophysical Research Letter 32, L20708. https://doi.org/10.1029/2005GL024233.
Lachniet, M.S., 2009. Climatic and environmental controls on speleothem oxygen-isotope values. Quat. Sci. Rev. 28 (5–6), 412–432. https://doi.org/10.1016/j.quascirev.2008.10.021. ISSN 0277-3791.
Lachniet, M., Bernal, J.P., Asmerom, Y., et al., 2012. A 2400 yr mesoamerican rainfall reconstruction links climate and cultural change. Geology 40, 259–262. https://doi.org/10.1130/g32471.1.
Lachniet, M.S., Asmerom, Y., Polyak, V., et al., 2017. Two millennia of Mesoamerican monsoon variability driven by Pacific and Atlantic synergistic forcing. Quat. Sci. Rev. 155, 100–113. https://doi.org/10.1016/j.quascirev.2016.11.012.
Lechleitner, F., Breitenbach, S., Rehfeld, K., et al., 2017. Tropical rainfall over the last two millennia: evidence for a low-latitude hydrologic seesaw. Science Report 7, 45809. https://doi.org/10.1038/srep45809.
Li, W., Li, L., Fu, R., et al., 2011. Changes to the North Atlantic subtropical high and its role in the intensification of summer rainfall variability in the southeastern United States. J. Clim. 24 (5), 1499–1506. https://doi.org/10.1175/2010JCLI3829.1.
Li, L., Li, W., Kushnir, Y., 2012. Variation of the North Atlantic subtropical high western ridge and its implication to Southeastern US summer precipitation. Clim. Dynam. 39, 1401–1412. https://doi.org/10.1007/s00382-011-1214-y.
Li, L., Li, W., Barros, A.P., 2013. Atmospheric moisture budget and its regulation of the summer precipitation variability over the Southeastern United States. Clim. Dynam. 41, 613–631. https://doi.org/10.1007/s00382-013-1697-9.
Ludwig, K.R., 2012. User's Manual for Isoplot 3.75. A Geochronological Toolkit for Microsoft Excel, vol. 5. Berkeley Geochronology Centre Special Publication No., pp. 1–71. http://www.bgc.org/isoplot.htm
Ludwig, K.R., Paces, J.B., 2002. Uranium-series dating of pedogenic silica and carbonate, Crater Flat, Nevada. Geochem. Cosmochim. Acta 66, 487–506.
Magaña, V., Amador, J.A., Medina, S., 1999. The midsummer drought over Mexico and Central America. J. Clim. 12, 1577–1588. https://doi.org/10.1175/1520-0442(1999)012<1577:TMDOMA>2.0.CO;2.
Magaña, V.O., Vázquez, J.L., Pérez, J.L., et al., 2003. Impact of El Niño on precipitation in Mexico. Geofisc. Int. 42 (3), 313–330. https://doi.org/10.22201/igeof.00167169p.2003.42.3.949.
Mann, M.E., Zhang, Z., Rutherford, S., Bradley, R.S., Hughes, M.K., Shindell, D., Ammann, C., Faluvegi, G., Ni, F., 2009. Global signatures and dynamical origins of the Little Ice Age and Medieval Climate Anomaly. Science 326, 1256–1260.
Medina-Elizalde, M., Burns, S.J., Lea, D.W., 2010. High resolution stalagmite climate record from the Yucatán Peninsula spanning the Maya terminal classic period. Earth Planet Sci. Lett. 298 (Issues 1–2), 255–262. https://doi.org/10.1016/j.epsl.2010.08.016. ISSN 0012-821X.
Mestas-Nuñez, A.M., Enfield, D.B., Zhang, C., 2007. Water vapor fluxes over the IntraAmericas Sea: seasonal and interannual variability and associations with rainfall. J. Clim. 20 (9), 1910–1922. https://doi.org/10.1175/JCLI4096.10.
Metcalfe, S.E., Jones, M.D., Davies, S.J., et al., 2010. Climate variability over the last two millennia in the North American Monsoon region, recorded in laminated lake sediments from Laguna de Juanacatlán, Mexico. Holocene 20 (8), 1195–1206. https://doi.org/10.1177/0959683610371994.
Murray-Tortarolo, G.N., 2021. Seven decades of climate change across Mexico. Atmósfera 34 (2), 217–226. https://doi.org/10.20937/atm.52803.
Ortega, P., Lehner, F., Swingedouw, D., et al., 2015. A model-tested North Atlantic Oscillation reconstruction for the past millennium. Nature 523, 71–74. https://doi.org/10.1038/nature14518.
Paton, C., Hellstrom, J., Paul, B., et al., 2011. Iolite: freeware for the visualisation and processing of mass spectrometric data. Journal of Analytical Atomic Spectrometry 26 (12), 2508–2518. https://doi.org/10.1039/c1ja10172b.
Peristykh, A.N., Damon, P.E., 2003. Persistence of the Gleissberg 88-year solar cycle over the last 12,000 years: evidence from cosmogenic isotopes. JOURNAL OF GEOPHYSICAL RESEARCH 108 (A1), 1003. https://doi.org/10.1029/2002JA009390.
Richey, J.N., Poore, R.Z., Flower, B.P., et al., 2009. Regionally coherent little ice age cooling in the atlantic warm pool. Geophysical Research Letter 36, L21703. https://doi.org/10.1029/2009GL040445.
Rind, D.H., 1998. Latitudinal temperature gradients and climate change. J. Geophys. Res. 103 (D6), 5943–5971. https://doi.org/10.1029/97JD03649.
Scholz, D., Hoffmann, D.L., 2011. StalAge–An algorithm designed for construction of speleothem age models. Quat. Geochronol. 6 (3–4), 369–382. https://doi.org/10.1016/j.quageo.2011.02.002.
Schultz, D.M., Bracken, W.E., Bosart, L.F., 1998. Planetary-and synoptic-scale signatures associated with Central American cold surges. Mon. Weather Rev. 126 (1), 5–27. https://doi.org/10.1175/1520-0493(1998)126<0005:PASSSA>2.0.CO;2.
Sinclair, D.J., 2011. Two mathematical models of Mg and Sr partitioning into solution during incongruent calcite dissolution: implications for dripwater and speleothem studies. Chem. Geol. 283, 119–133. https://doi.org/10.1016/j.chemgeo.2010.05.022.
Stahle, D.W., Cook, E.R., Burnette, D.J., et al., 2016. The Mexican Drought Atlas: tree-ring reconstructions of the soil moisture balance during the late prehispanic, colonial, and modern eras. Quat. Sci. Rev. 149, 34–60. https://doi.org/10.1016/j.quascirev.2016.06.018. ISSN 0277-3791.
Sud, Y.C., Walker, G.K., Lau, K.-M., 1999. Mechanisms regulating sea-surface temperatures and deep convection in the tropics. Geophys. Res. Lett. 26, 1019–1022.
Sun, Y., Bekker, M.F., DeRose, R.J., et al., 2017. Statistical treatment for the wet bias in tree-ring chronologies: a case study from the Interior West, USA. Environ. Ecol. Stat. 24, 131–150. https://doi.org/10.1007/s10651-016-0363-x.
Taylor, S.R., Mclennan, S.M., 1985. The Continental Crust: its Composition and Evolution. An Examination of the Geochemical Record Preserved in Sedimentary Rocks. Blackwell Scientific publications.
Thirumalai, K., Quinn, T.M., Okumura, Y., Richey, J.N., Partin, J.W., Poore, R.Z., Moreno-Chamarro, E., 2018. Pronounced centennial-scale Atlantic Ocean climate variability correlated with Western Hemisphere hydroclimate. Nat. Commun. 9 (1), 392.
Wang, C., 2007. Variability of the Caribbean low-level jet and its relations to climate. Clim. Dynam. 29, 411–422. https://doi.org/10.1007/s00382-007-0243-z.
Wogau, K.H., Arz, Helge W., Böhnel, Harald N., Nowaczyk, Norbert R., Park, Jungjae, 2019. High resolution paleoclimate and paleoenvironmental reconstruction in the Northern Mesoamerican Frontier for Prehistory to Historical times. Quat. Sci. Rev. 226, 106001. https://doi.org/10.1016/j.quascirev.2019.106001. ISSN 0277-3791.
Wright, K.T., Johnson, K.R., Bhattacharya, T., Marks, G.S., McGee, D., Elsbury, D., et al., 2022. Precipitation in Northeast Mexico primarily controlled by the relative warming of Atlantic SSTs. Geophys. Res. Lett. 49, e2022GL098186. https://doi.org/10.1029/2022GL098186.
Yan, H., Sun, L., Wang, Y., et al., 2011. A record of the Southern Oscillation Index for the past 2,000 years from precipitation proxies. Nature Geosci 4, 611–614. https://doi.org/10.1038/ngeo1231.
Yun, K.S., Lee, J.Y., Timmermann, A., et al., 2021. Increasing ENSO–rainfall variability due to changes in future tropical temperature–rainfall relationship. Commun Earth Environ 2, 43. https://doi.org/10.1038/s43247-021-00108-8.